METABOLISM AND BIODISTRIBUTION OF MODIFIED EXTRACELLULAR VESICLES IN COLORECTAL CANCER MODELS

A THESIS
SUBMITTED TO THE FACULTY OF THE
UNIVERSITY OF MINNESOTA BY

BILVA NITIN BURKULE

IN PARTIAL FULFILLMENT OF THE REQUIREMENTS
FOR THE DEGREE OF
MASTER OF SCIENCE

DR. SUBBAYA SUBRAMANIAN, ADVISER

JULY 2021

Acknowledgements

I wish to express my sincere gratitude to my advisor Dr. Subbaya Subramanian for his valuable guidance and support throughout my graduate research work. He provided me with an opportunity to build my scientific knowledge in a friendly, creative, supportive and highly enthusiastic laboratory environment. I am deeply motivated by his vision and mentoring style.

I would really like to thank my lab mates Xianda Zhao, Angelo Yuan, Dechen Wangmo, Travis Gates and Shawn Morris for teaching me new research techniques and for helping me design my experiments. I would like to thank Duha Alshareef, graduate student from Campbell laboratory for her guidance in designing and planning my experiments.

I am thankful to Dr. Cheuk Leung and Dr. Kaylee Schwertfeger for participating as my thesis committee members and reviewing my thesis document. I would like to really thank them for their constructive and insightful feedback related to my graduate research work.

I am thankful to my parents- Nitin Burkule and Sandhya Burkule for their unconditional love and support and for the sacrifices they made to help me achieve my goals. I am also thankful to my sister Snigdha Burkule for her guidance and support during my graduate studies.

Table of Contents

Table of Contents

List of figures

List of tables

Chapter 1: Effect of Metabolism of Modified Extracellular Vesicles on Colorectal cancer cells

1. Introduction

The term 'exosomes' was first discovered in 1981 in the form of shedding vesicles with 5' nucleotidase activity in normal and cancerous cells. They are nano-sized extracellular vesicles (EVs) which are small, lipid bilayer membrane vesicles with an average size ranging from 30-150 nm. EVs are derived from the luminal membrane of multivesicular bodies (MVBs), which are constitutively released by fusion with the cell membrane [1,2]. Tumor derived exosomes (TEVs) have been implicated in formation of pre-metastatic niche, metabolic reprogramming, formation of extracellular matrix, angiogenesis and immunosuppression.

'Metabolic reprogramming' is a recognized hallmark of cancer. A common feature of cancer cell metabolism is the ability to acquire necessary nutrients from a frequently nutrient-poor environment and utilize these nutrients to both maintain viability and build new biomass [3]. Alterations in intracellular and extracellular metabolites which induce cancer-associated metabolic reprogramming have a profound impact on tumor microenvironment. Cancer cells actively secrete exosomes that have the potential to exacerbate tumor growth and formation through metabolic remodelling [4]. TEVs targeting metabolic reprogramming could provide novel insights for developing therapeutic strategies for cancer. Recently, organoids have been introduced as complex model system to study the metabolic reprogramming induced by intracellular and intercellular communication in the tumor microenvironment. These models are more physiologically relevant to perform metabolic studies in cancer [5].

Due to size overlap between exosomes and microvesicles, the term extracellular vesicles (EVs) will be used to demonstrate our work. In this chapter, we will review the biogenesis, uptake and release mechanisms of EVs, their potential as diagnostic and therapeutic markers, metabolic mechanisms in colorectal cancer (CRC), metabolic reprogramming by CRC derived EVs and current organoid models utilized to study metabolism in CRC. Our approach is to determine the metabolic profile of modified

CRC cells. In the next step, we have developed an CRC organoid EV co-culture system to define the metabolic changes induced by EVs in CRC.

1.1 Biogenesis, release and uptake of exosomes

Exosomes originate from MVB [6,7]. To begin with, plasma membrane and cytosolic contents such as proteins, lipids, nucleic acids (for eg: DNA, RNA,mRNA) are endocytosed and transfer to the early endosomes. These early endosomes get accumulated into the intraluminal vesicles (ILVs) through inward budding. Due to their structural similarities containing ILVs are usually referred to as MVBs [8]. These early endosomes differentiate into late endosomes (MVBs) **[refer Fig.1]**. Then the late endosomes fuse with lysosomes causing their degradation or fuse with plasma membrane releasing exosomes into the extracellular space.

The endosomal sorting complex required for transport (ESCRT) machinery regulates exosome biogenesis [9] **[refer Fig.1]**. It is required for MVB formation because it separates the ubiquitinated intracellular cargos that are destined for endosomal degradation into MVBs. The ESCRT machinery consists of four ESCRT proteins: ESCRT-0,ESCRT-l,ESCRT-ll and ESCRT-III. Along with accessory proteins: VPS4, VTA1, ALG2 containing protein X (Alix 2). ESCRT-0 binds to ubiquitinated proteins, endosomal membrane recruits ESCRT-1 [tumor susceptibility gene 101 (tsg101)] and vps28. ESCRT-1 recruits ESCRT-11, together they facilitate the formation of reverse budding in MVBs and formation of cytosolic cargos [10]. Usually, ESCRT subunits are released into the cytosol but some accessory proteins such as ALIX and TSG101 remain in the exosomes.

There are certain mechanisms associated with release of exosomes **[refer Fig.1].** For instance, The reduction of expression of Sirutin-1 (SIRT1) expression decreases the levels of lysosomal vacuolar type H^+ ATPase proton pump (ATP6V1A) resulting in enlargement of MVBs fused with plasma membrane to release exosomes [11]. The pseudokinase mixed lineage kinase domain like (MLKL) which triggers necroptosis upon phosphorylation of RIPK3 a protein kinase triggers the release of exosomes [12]. Pyruvate kinase type M2 (PKM2) promotes exosome release from tumour cells by phosphorylating synaptosome associated protein 23 (SNAP23), which enables the formation of the soluble N-ethylmaleimide sensitive fusion factor attachment protein receptor (SNARE) complex to allow exosome release [13]. Again, exosomes that are

released into the body fluids or tumour microenvironment are taken up by receiver cells by certain mechanisms. They can also be taken up by receiver cells through direct fusion of their membrane in different manners such as lipid raft, calveolae, and clathrin dependent endocytosis, 3icropinocytosis and phagocytosis. Recently, Dynamin 2 has been reported to be an essential regulator of phagocytosis and exosome uptake [14]. From a broader perspective, the knowledge of biogenesis, release and uptake requires further investigation.

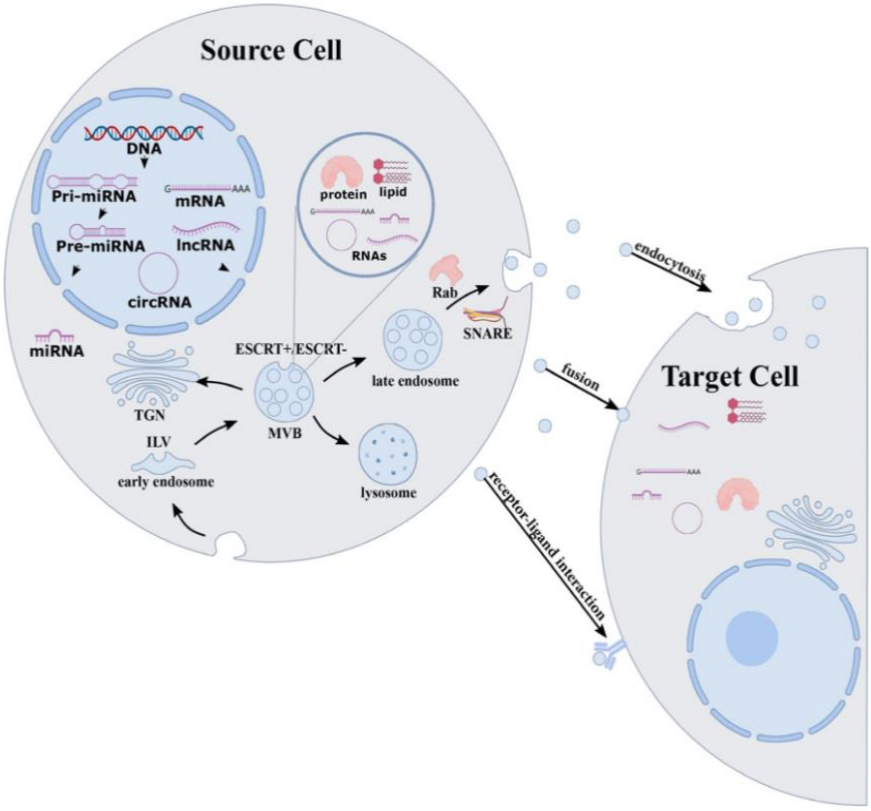

Fig. 1: Schematic representation of biogenesis, release and uptake of exosomes. From (Yue *et. Al,*[15]).

1.2 Exosomes as potential therapeutic and diagnostic markers in cancer

Exosomes have been identified as promising therapeutic and diagnostic targets in cancer. Exosomes could be utilized as promising therapeutic agents in regenerative medicine and tissue repair and modulation of immune response in a desired direction either by antigen specific or unspecific events [16] **[refer Fig.2].** An instance of therapeutically targeting exosomes is targeting the exosomal membrane bound PD-L1.

PD-L1 is a membrane bound ligand that binds to its receptor PD-1 on surface of T cell to inhibit their activation [17]. Hence, PD1–PDL1 pathway inhibitors increases, both as single agents and in combination therapy, could clinically serve as useful biomarkers and maximize patient benefit in CRC. The immunomodulatory effects of extracellular vesicles can include antigen transfer and presentation: for example, as used in anticancer vaccines and in the elimination of infections by priming specific $CD8^+$ T cells [16].

Exosomes can be used as prognostic markers for early detection of tumors. TEVs have endogenous tumor antigens, thus, can be utilized to elucidate anti-tumor immune response through presenting the antigens to antigen presenting cells, such as dendritic cells [7,18].

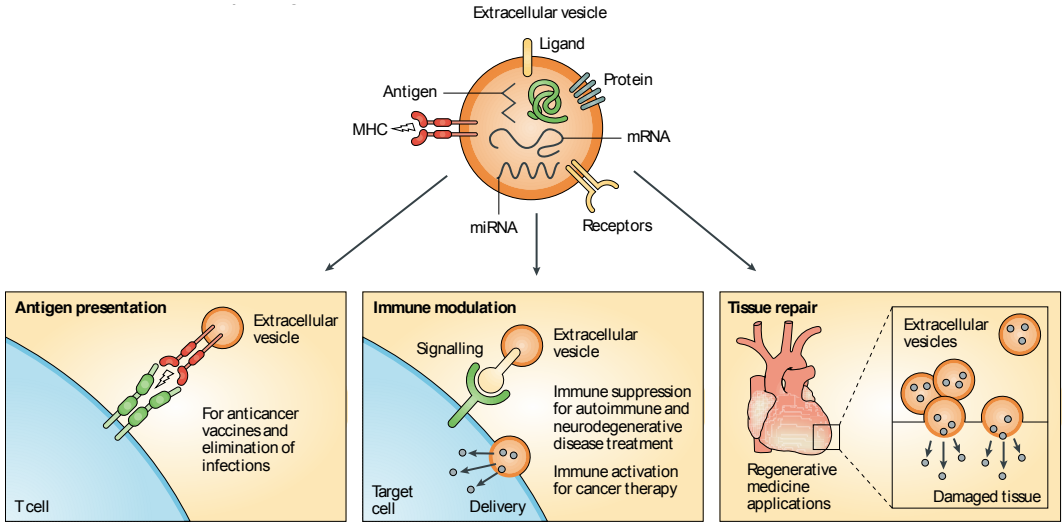

Fig. 2: Exosomes as therapeutic agents. From (*El Andaloussi et. Al* [16]).

1.3 Metabolic mechanisms in Colorectal Cancer

Metabolism is a sum of chemical reactions that a cell undergoes to satisfy its energy demands. It is a balance between anabolism and catabolism, resulting in cells producing energy in the form of ATP. According to the Warburg effect, cancer cells consume more glucose to produce energy via biosynthetic pathways as compared to normal cells [19]. Cancer cells exhibit the 'Warburg Phenotype'. In this phenomenon, in the presence of oxygen cancer cells preferentially shift their metabolism towards glycolysis followed by OXPHOS. This state of glycolysis is known as 'aerobic glycolysis'. Till

date, studies in CRC metabolism have identified that, primary and metastatic CRC tumors often exhibit higher glucose consumption than surrounding normal tissue [20]. The common metabolic mechanisms in CRC like other cancer types are: Glycolysis, Tricarboxylic acid (TCA) cycle, Glutaminolysis, One carbon metabolism and Oxidative Phosphorylation (OXPHOS) **[refer Fig. (3)]**.

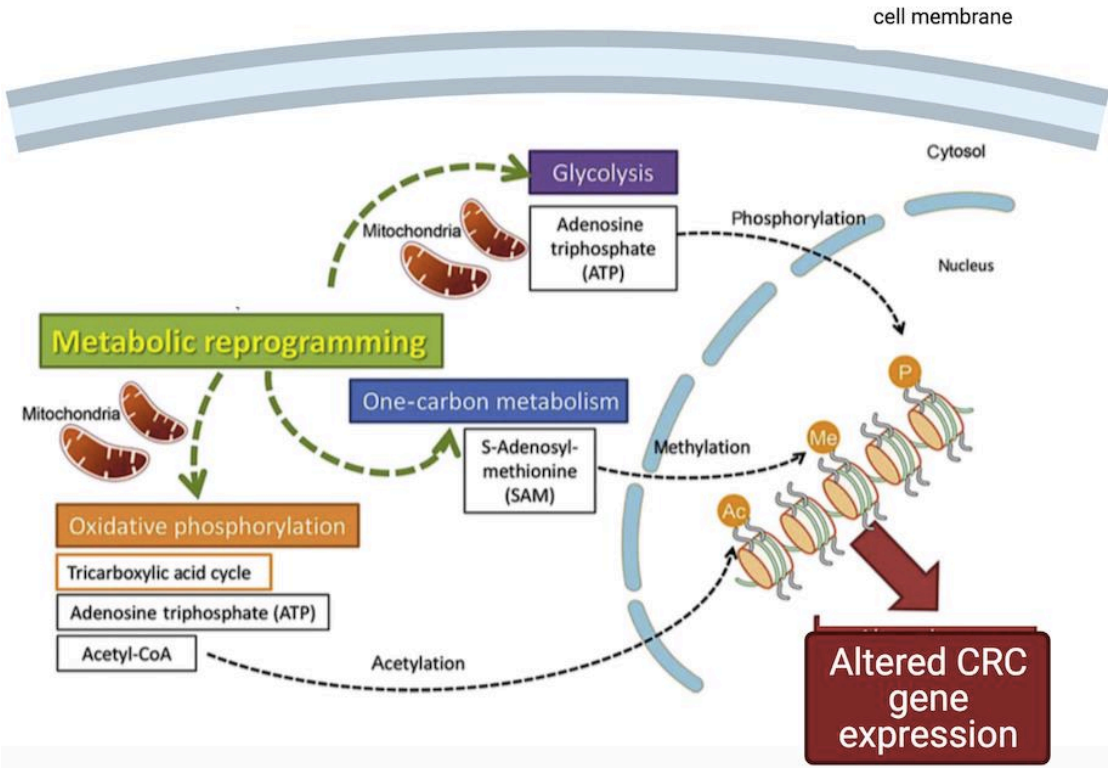

Fig. 3: Metabolic mechanisms in Colorectal Cancer. From (Hagland *et.,al* [26]).

In Glycolysis, glucose is oxidized to pyruvate, as a result of this reaction macromolecule intermediates formed support cell growth. Pyruvate is finally reduced to lactate by lactate dehydrogenase and is finally secreted out of the cell via monocarboxylate transporter (MCT4) [21]. The end product of glycolysis is channelled through to TCA cycle (Kreb's cycle) and goes through ETC by getting converted to acetyl coenzyme A (Acetyl CoA). Acetyl CoA reduces nicotinamide adenine dinucleotide (NAD^+) and flavin adenine dinucleotide (FAD) to NADH and FADH2. These electron carriers create a proton gradient across the mitochondrial membrane and produce ATP by the electron transport chain (ETC). Since glycolytic intermediates are driven towards biosynthetic pathways, cancer cells utilize glutamine to replenish the

TCA cycle [22]. Glutamine is deaminated to glutamate by glutaminase. Glutamate is further converted to α-ketoglutarate (α-KG). α-KG can be employed to synthesize amino acids, lipids and generate ATP followed by OXPHOS. Moving forward, one carbon metabolism is responsible for increased nucleotide and fatty acid synthesis by proliferating CRC cells. 5-methyltetrahydrofolate, an intermediate of this pathway causes adenylation of methionine to form S-adenosylmethionine (SAM) [23]. SAM initiates DNA methylation leading to altered CRC gene expression. It is now thought that, cancer cells utilize the TCA cycle (fuelled by pyruvate, lactate, glutamine and fatty acids) followed by OXPHOS to generate ATP [24,25]. OXPHOS generates higher ATP molecules as compared to glycolysis.

1.4 Metabolic reprogramming by colorectal cancer derived extracellular vesicles

Recently, EVs have been identified as the crucial signaling mediators in the tumor microenvironment. Accumulated evidence indicates that EVs may transfer biologically functional molecules to the recipient cells, which facilitate cancer progression, angiogenesis, metastasis, drug resistance, and immunosuppression by reprogramming the metabolism of cancer cells [4]. Some reported studies delineating the metabolic reprogramming mediated by CRC EVs are as follows: CRC derived small EVs can transport miRNA-122 that can reduce glucose uptake in normal fibroblasts, and other proteins and enzymes that influences glycolysis in cancer cells [19]. Another study demonstrated that small EVs derived from CRC mutant KRAS-expressing cells contain proteins and enzymes involved in metabolism and glycolysis and can enhance the growth of wild type KRAS cells [27]. Wang *et. al* discovered exosomal ciRS-122 from the serum of oxaliplatin-resistant CRC patients and oxaliplatin- sensitive patients. Compared with the oxaliplatin-sensitive group, the oxaliplatin-resistant group had higher ciRS-122 expression levels in the exosomes. Moreover, Exosomal ciRS-122 derived from drug-resistant colorectal cancer cells could enhance the glycolysis to reduce drug sensitivity in drug-sensitive cells, which revealed that exosomal ciRS-122 could regulate metabolism to favor tumor drug resistance [28]. According to this biological characteristic of exosomes, Shu *et. al* discovered that exosomes transferred with miRNA inhibitors could reverse the exosome-mediated metabolic reprogramming, which could reduce the risk of tumor metastasis [29].

1.5 Organoid models for studying metabolism

Organoids can be developed from different tissues including tumours, representing the cell population and spatial organization of the tissue of origin [5]. **Fig. 4** enlists the advantages of utilizing organoids in metabolic research: Organoids can be generated from several tissues, allowing the comparison of several variables between different species, different tissues within the same species or tumour *vs.* healthy tissue. Furthermore, since organoids arise from stem cells, they represent the entire population of the tissue of origin. They can be also used in co-culture tissue. 3D culture of organoids allows the development of the hypoxic core usually observed within tumour samples.

Organoids can also be used with microfluidics technology, allowing the generation of for example, artificial vasculature. The ability to genetically manipulate organoids, can introduce a better understanding or disease development from earlier steps. Finally, the generation of both tumour and healthy organoids from the same donor contributes to the development of personalized medicine and thus, drug development and high throughput screening.

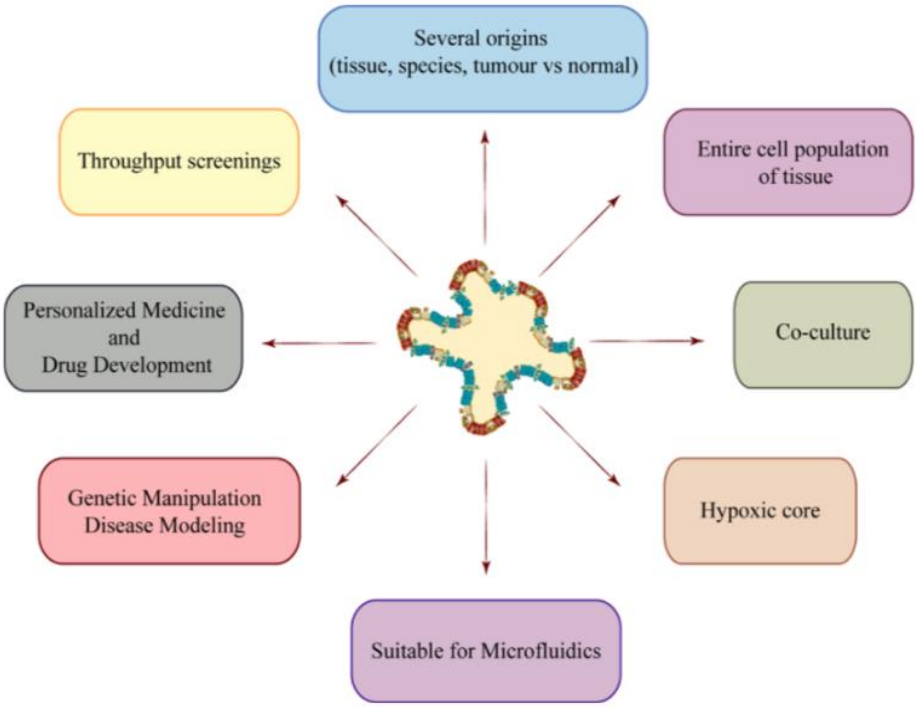

Fig. 4: Advantages of organoids in metabolic research. From (*C. Silva-Almeida, et. al* [5]).

In a study published by Bas *et.al*, mouse intestinal crypt organoids from 8 month old C57Bl/6 mice were cultured *ex-vivo* to test the mitochondrial and glycolytic capability of these organoids to study crypt organoid metabolism [30]. The metabolic assays described here provides a possible evaluation of relative risk for CRC development and for early detection of CRC, its biochemical and molecular dissection and potential modulation. Our approach of developing an organoid EV co-culture system is presently not reported in literature.

1.6 Seahorse extracellular flux analysis

The seahorse extracellular flux assay measures two major energy producing pathways of the cell - mitochondrial respiration (oxygen consumption rate = OCR) and glycolysis (extracellular acidification rate = ECAR). These findings shall enhance our understanding of cellular function, activation, proliferation and disease etiology. We plan to use the Cell Energy Phenotype test to determine the metabolic profile of CRC cell variants: Wild type (WT CRC) cells, microRNA control CRC cells (MZ Ctrl) with microRNA424 knocked down CRC cells (MZ424 CRC cells).

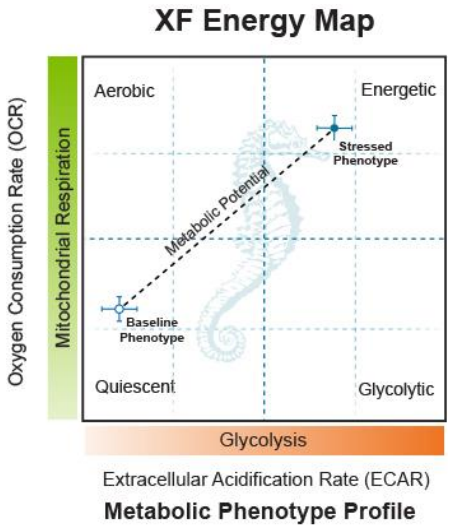

Fig. 5: Seahorse XF Cell Energy Phenotype Profile. The relative utilization of the two energy pathways (mitochondrial respiration and glycolysis) of a cell population is determined under both baseline (Baseline Phenotype) and stressed (Stressed Phenotype) conditions. The response to an induced energy demand is their Metabolic Potential. (From [31]).

The cell energy phenotype test Reveals 3 key parameters of cell metabolism **[refer Fig. 5]:**

1. Baseline phenotype: OCR and ECAR of cells at starting assay conditions

2. Stressed phenotype: OCR and ECAR of cells under energy demand [in the presence of stressor mix (Oligomycin and FCCP)]

3. Metabolic phenotype: Measure of cells ability to meet an energy demand via respiration and glycolysis (metabolic potential of cell)

2. Rationale and Aim

CRC is the third most prevalent cancer in the world. The lifetime risk for developing CRC is 1 in 23 (4.3%) for men and 1 in 25 (4.0%) for women. Recent studies in metastatic CRC have demonstrated that different mechanisms associated with immune regulation such as T cell co-stimulation, immune evasion could help in understanding and improving anti-tumor response [32]. Recent studies have shown that EVs play a critical role in intercellular communication in tumor microenvironment [1].

Previous research in our lab has demonstrated that tumor derived exosomes (TEVs) negatively regulate the immunity in CRC and CRC cells secreted EVs with microRNA 424 (miR-424) suppressed the CD28-CD80/86 costimulatory pathway in tumor infiltrating T cells and dendritic cells [32]. However, EVs without immunosuppressive miR-424 (**modified EVs**) enhanced the anti-tumour response in CRC tumor mouse model. Hence, we plan to utilize modified EVs for our present studies.

Previous studies have shown that CRC cells demonstrate the “Warburg” metabolic phenotype [20]. For instance, primary and metastatic CRC tumours often exhibit higher glucose consumption than surrounding normal intestinal tissue. In an immune system, metabolic programs of different CRC cells are associated with re-programming the immunity and hence EVs derived from these cell subsets could be responsible for re-programming the immunity in CRC [19]. Knowledge of how modified EVs regulate glucose metabolism and oxygen consumption will be useful in the context of identifying drug targets for different biochemical pathways and developing newer therapeutic strategies for CRC patients.

To determine the metabolic changes in CRC cells stably expressing anti-miR-424, we will test the metabolic profile of miR-424 knockdown mouse CRC cells with MSS and MSI phenotypes using wild type (WT) CRC cells and vector control (miRzip = MZ) expressing CRC cells as controls. Moving forward, we plan to evaluate the metabolic profiles of mouse CRC and normal colon derived organoids using an in vitro EV CRC co-culture model system. We will co-culture modified EVs and control CRC cell derived EVs with CRC organoids and compare their metabolic profiles. The analysis of mitochondrial respiration and glucose metabolism of cells will define the metabolic changes induced by modified EVs in CRC organoids and the effect of modified EVs on CRC cells.

3. Material and methods

3.1 Cell culture

A murine colon cancer cell line CT26 transduced with anti-miR424/322 expression lentivector (CT26 MZ424) was established in the lab previously. The anti-miR424/322 expression lentivector was procured from SIGMA ALDRICH. The murine colon cancer cell lines: CT26 WT, CT26 cells transduced with scrambled microRNA (CT26 MZ) and CT26 MZ424 were cultured in RPMI 1640 media supplemented with 10% FBS and 1% antibiotics. Similarly, murine colon cancer cell lines: MC38 WT, MC38 cells transduced with scrambled microRNA (MC38 MZ) and MC38 MZ424 cells [MC38 cell line transduced with anti-miR-424/322 lentiviral vector (SIGMA ALDRICH)] established previously in the lab were cultured in DMEM media supplemented with 10% FBS and 1% antibiotics.

3.2 Seahorse extracellular flux analysis

A day before the assay, the cartridge for Agilent seahorse XF 24 well plate is hydrated using the Agilent seahorse XF calibrant. The cartridge was placed in 37°C incubator overnight. 250k cells were plated in triplicates in the Agilent seahorse XF cell culture 24 well plate.

On the day of assay, Agilent seahorse XF base media was prepared by adding 1 mM seahorse XF pyruvate, 2 mM seahorse XF glutamine and 10 mM seahorse XF glucose

to it. The pH was adjusted up to 7.4 and the media was warmed by storing in the 37°C incubator. The cells in the Agilent seahorse XF cell culture 24 well plate were washed by removing the growth medium. Initially, PBS was added to the wells and cells were washed by gently shaking the plate. The PBS was removed and replaced by adding 500µL of growth media to each well. The Agilent seahorse XF cell culture 24 well plate was placed back in the 37°C incubator. 56µL of stressor mix comprising of 10µM Oligomycin and 5µM FCCP in Agilent seahorse XF media was loaded in the Agilent seahorse XF cartridge. The cartridge was calibrated for 30 minutes using the Agilent seahorse extracellular XFe24 analyzer. After 30 minutes, the calibrant containing 24 well plate was replaced with the Agilent seahorse XF cell culture 24 well plate. The data was acquired using the Agilent seahorse extracellular XFe24 analyzer and analyzed using the wave 2.0 software.

3.3 Mouse CRC organoid culture

Previously established organoids from colon polyps derived from C57Bl/6 mice from Charles River Laboratory were used for the study. Organoid base media was prepared by combining Advanced DMEM and L-WRN cell supernatant (consisting of R-Spondin, Noggin and EGF growth factors) in 1:1 ratio. In order to prepare the organoid media, 10µM Y-2763,1mM N-Acetylcysteine, 1 X of each N2 and B27 supplements and primocin were further added to the base media. These organoids were cultured in the organoid media.

3.4 EV Isolation

Before EV isolation, CT26 WT, CT26 MZ Ctrl. and CT26 MZ424 cells were cultured until they reached an approximate confluency of 80%. The media for CT26 WT, CT26 MZ Ctrl. and CT26 MZ424 cells was replaced with RPMI 1640 media supplemented with 10% EV depleted FBS and 1% antibiotics one day before the isolation. EVs from each cell lines were harvested and purified by centrifuging cell culture supernatant at different speeds to remove cells and cells debris: 300 x g for 10 min, 2000 x g for 10 min, and 10000 x g for 30 min. To concentrate the samples, 15mL Amicon Ultra filter tubes (MilliporeSigma) were used and centrifuged at 3200 x g for 30 min. Concentrated media was; then, ultracentrifuged twice at 100000 x g for 70 min. The resulted pellets

were resuspended in 120µl PBS for each cell type, then protein concentration was measured using micro BCA protein assay kit (Thermo Fisher Scientific).

3.5 EV organoid co-culture system

EVs from murine CRC cell lines were isolated as per the EV isolation protocol described **in section 3.4**. 50k mouse CRC organoid cells were plated in triplicates in the seahorse XF cell culture 24 well plate. A co-culture system was developed by adding the isolated EVs to the mouse CRC organoids in the seahorse XF cell culture 24 well plate. This plate was kept in the 37°C incubator for 48 hours. After 48 hours, the metabolic profile of EVs was analyzed using the Agilent seahorse extracellular flux XFe24 analyser as per the protocol described in **section 3.2.**

4. Results

We compared the metabolic profiles of murine colon cancer CT26 WT cells and CT26 CT26 MZ Ctrl. (CT26 MZ) with CT26 MZ424 cells by utilizing the cell energy phenotype test in the seahorse extracellular flux analyzer. Similarly, we compared the metabolic profiles of murine colon cancer MC38 WT and MC38 MZ Ctrl. (MC38 MZ) with MC38 MZ424 cells. Moreover, we co-cultured modified EVs with mouse CRC organoids to compare their metabolic profiles with CT26 WT EVs and CT26 MZ Ctrl. EVs co-cultured with mouse CRC organoids.

4.1 Cell density optimization of CT26 cell phenotypes

To identify the best cell number for conducting the seahorse extracellular flux assay, we plated the CT26 cell variants: CT26 WT and CT26 MZ424 cells in three different concentrations. We plated 250k, 500k and 750k cells in triplicates for each of the CT26 cell variants (CT26 WT and CT26 MZ424 cells) in the seahorse cell culture 24 well plate.

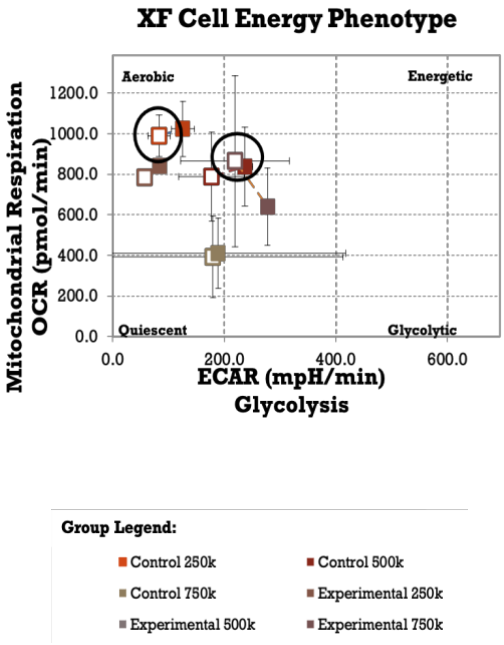

Fig. 6: Cell density optimization of CT26 cell phenotypes. Control cells represent CT26 WT cells and experimental cells represent CT26 MZ424 cells. The encircled plots represent the metabolic potential of CT26 WT and CT26 MZ424 each with a cell number of 250k.

Group name	Baseline OCR/ECAR ratio
Control 250k	**11.90**
Control 500k	4.45
Control 750k	2.18
Experimental 250k	**13.76**
Experimental 500k	4.38
Experimental 750k	3.95

Table 1: Baseline OCR/ECAR ratios of CT26 cell phenotypes. In table 1, the highlighted group name represents the baseline OCR/ECAR ratios of CT26 WT and CT26 MZ424 each with a cell number of 250k which was selected for seahorse extracellular flux analysis.

Based on the data, we selected 250k as the best cell number to proceed with the seahorse extracellular flux assay to assess the metabolic profiles of CT26 cell variants. Since for both the cell types i.e. CT26 WT (control group) and CT26 MZ424 cells (experimental

group), the baseline OCR/ECAR ratio is the highest as compared to the other two control and experimental groups **[refer Fig. (6) and Table 1).** The baseline OCR/ECAR ratio for CT26 WT cells is 11.90 and CT26 MZ424 cells is 13.76.

4.2 Metabolic profiling of CT26 cell phenotypes

To gain insights into the metabolic potential of CT26 MZ424 cells we performed the cell energy phenotype test utilizing the seahorse extracellular flux analyzer. A day before the assay, we plated 250k cells in triplicates for each of the CT26 cell variants (CT26 WT, CT26 MZ Ctrl. and CT26 MZ424) in the seahorse cell culture 24 well plate.

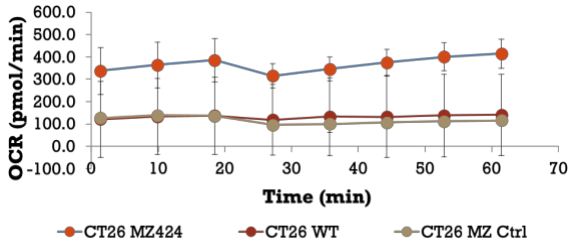

Fig. (7a) OCR Metabolic curve for CT26 cell phenotypes

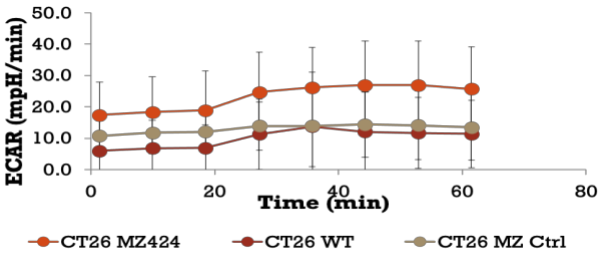

Fig. (7b) ECAR metabolic curve for CT26 cell phenotypes

Fig. 7: Cell energy phenotype test of CT26 cell variants

Group Name	Baseline ECAR	Baseline ECAR StdDev	Stressed ECAR	Stressed ECAR StdDev	Metabolic Potential (% Baseline ECAR)	Metabolic Potential StDev (ECAR)
CT26 MZ Ctrl.	12.12	12.61	23.02	13.99	189.89	12.40
CT26 WT	19.82	7.43	47.17	26.43	238.05	7.98
CT26 MZ424	7.73	5.48	33.74	12.21	436.42	40.15

Table 2: OCR values for CT26 cell phenotypes. In table 2, OCR data summary for CT26 WT, CT26 MZ Ctrl. and CT26 MZ424 cells. Represents the % metabolic potential (stressed OCR/baseline OCR*100) in terms of OCR.

Group name	Baseline OCR	Baseline OCR StdDev	Stressed OCR	Stressed OCR StdDev	Metabolic Potential (% Baseline OCR)	Metabolic Potential StDev (OCR)
CT26 MZ Ctrl	198.69	96.07	184.86	108.42	93.04	10.13
CT26 WT	350.38	173.46	384.20	183.00	109.65	5.29
CT26 MZ424	127.70	6.82	135.92	17.98	106.43	4.66

Table 3: ECAR values for CT26 cell phenotypes. In table 3, ECAR data summary for CT26 WT, CT26 MZ Ctrl. and CT26 MZ424 cells. Represents the % metabolic potential (stressed ECAR/baseline ECAR*100) in terms of ECAR

Figs. (7a) and (7b) depict that the OCR and ECAR levels of CT26 MZ424 cells are higher as compared to the CT26 WT and CT26 MZ Ctrl cells. The OCR based metabolic potential of CT26 MZ424 cells is 109.95% which is higher than CT26 WT and CT26 MZ Ctrl. cells having metabolic potential values as 106.43% and 93.04% respectively **[refer table 2].** On the contrary, ECAR based metabolic potential of CT26 WT cells is 436.42% which is higher than CT26 MZ424 cells and CT26 MZ Ctrl. cells with metabolic potential values of 238.05% and 189.89% respectively **[refer table 3]**.

In order to study if the metabolic activity of murine colon cancer CT26 cell variants is higher than normal cells. A day before the assay, we plated 250k cells of CT26 cell

variants and NIH-3T3 fibroblasts in triplicates. We compared the metabolic profiles of CT26 cell variants with NIH-3T3 fibroblasts by utilizing the cell energy phenotype test in the seahorse extracellular flux analyzer.

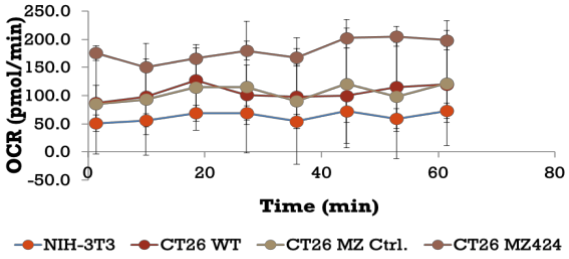

Fig. (8a) OCR metabolic curve for CT26 cell phenotypes and NIH-3T3 fibroblasts

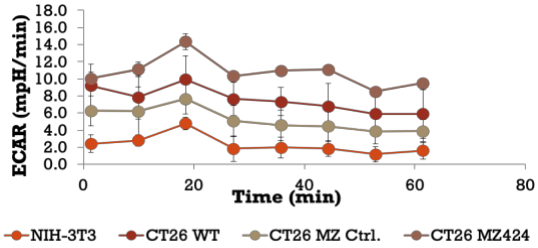

Fig. (8b) ECAR metabolic curve for CT26 cell phenotypes and NIH-3T3 fibroblasts

Fig. 8: Cell energy phenotype test of CT26 cell variants and NIH-3T3 fibroblasts

Group Name	Baseline OCR	Baseline OCR StdDev	Stressed OCR	Stressed OCR StdDev	Metabolic Potential (% Baseline OCR)	Metabolic Potential StDev (OCR)
CT26 MZ Ctrl.		13.95	36.62	13.73	110.75	12.40
CT26 MZ424	99.68	57.31	123.08	78.90	119.47	7.98
CT26 WT	95.45	76.28	89.99	110.29	93.05	40.15
NIH-3T3 fibroblasts	80.47	8.80	85.81	17.42	106.63	17.66

Table 4: OCR values for CT26 cell phenotypes and NIH-3T3 fibroblasts. In Table 4, OCR data summary for CT26 WT, CT26 MZ Ctrl.,CT26 MZ424 and NIH-3T3 fibroblasts. Represents the % metabolic potential (stressed OCR/baseline OCR*100) in terms of OCR.

Group Name	Baseline ECAR	Baseline ECAR StdDev	Stressed ECAR	Stressed ECAR StdDev	Metabolic Potential (% Baseline ECAR)	Metabolic Potential StDev (ECAR)
CT26 MZ Ctrl.	7.64	0.72	5.08	1.48	65.70	13.96
CT26 MZ424	8.61	2.73	6.65	2.67	75.87	7.03
CT26 WT	9.94	1.76	7.64	1.80	76.52	9.08
NIH-3T3 fibroblasts	4.77	0.92	1.97	0.03	42.34	7.83

Table 5: ECAR values for CT26 cell phenotypes and NIH-3T3 fibroblasts. In table 5, ECAR data summary for CT26 WT, CT26 MZ Ctrl., CT26 MZ424 and NIH-3T3 fibroblasts. Represents the % metabolic potential (stressed ECAR/baseline ECAR*100) in terms of ECAR.

Figs. (8a) and (8b) depict that the OCR and ECAR values of CT26 cell variants are higher than NIH-3T3 fibroblasts. The OCR based metabolic potential values for CT26 WT, CT26 MZ Ctrl. and CT26 MZ424 are 93.05%, 110.75% and 119.47% respectively and for NIH-3T3 fibroblasts is 106.63% **(refer table 4).** The ECAR based metabolic potential values of CT26 cell variants is significantly higher than NIH-3T3 fibroblasts. The ECAR based metabolic potential values of CT26 WT, CT26 MZ Ctrl. and CT26 MZ424 are 76.52%, 65.70% and 75.87% respectively and for NIH-3T3 fibroblasts is 42.34% **(refer table 5).**

4.3 Metabolic profiling of MC38 cell phenotypes and NIH-3T3 fibroblasts

In order to compare the metabolic characteristics of murine colon cancer CT26 cell variants with another murine colon cancer cell line, we tested the metabolic profile of MC38 cell phenotypes. Additionally, to check if the metabolic activity of MC38 cell variants is higher than normal cells, we incorporated the NIH-3T3 fibroblasts in our study.

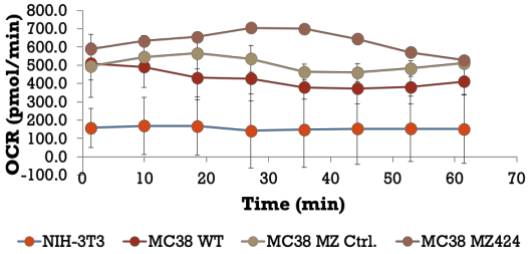

Fig. (9a) OCR metabolic curve for MC38 cell phenotypes and NIH-3T3 fibroblasts

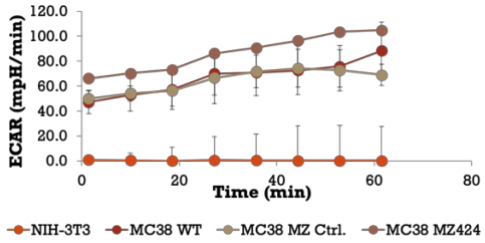

Fig. (9b) ECAR metabolic curve for MC38 cell phenotypes and NIH-3T3 fibroblasts

Fig. 9: Cell energy phenotype test of MC38 cell variants and NIH-3T3 fibroblasts.

Group Name	Baseline OCR	Baseline OCR StdDev	Stressed OCR	Stressed OCR StdDev	Metabolic Potential (% Baseline OCR)	Metabolic Potential StDev (OCR)
MC38 MZ Ctrl.	1017.17	158.20	962.90	201.98	94.18	4.98
MC38 MZ424	982.29	121.83	1055.68	119.77	107.58	2.18
MC38 WT	949.79	83.81	937.41	73.55	98.76	1.86
NIH-3T3 fibroblasts	167.64	24.35	153.05	25.49	91.41	10.61

Table 6: OCR values for MC38 cell phenotypes and NIH-3T3 fibroblasts. In table 6, OCR data summary for MC38 WT, MC38 MZ Ctrl., MC38 MZ424 and NIH-3T3 fibroblasts. Represents the % metabolic potential (stressed OCR/baseline OCR*100) in terms of OCR.

Group Name	Baseline ECAR	Baseline ECAR StdDev	Stressed ECAR	Stressed ECAR StdDev	Metabolic Potential (% Baseline ECAR)	Metabolic Potential StDev (ECAR)
MC38 MZ Ctrl.	101.48	11.03	133.67	27.78	131.19	19.98
MC38 MZ424	109.67	13.28	157.03	22.85	143.30	14.87
MC38 WT	125.68	15.14	194.32	8.64	156.60	25.35
NIH-3T3 fibroblasts	0.02	0.36	0.66	0.66	-499.47	1158.10

Table 7: ECAR values for MC38 cell phenotypes and NIH-3T3 fibroblasts. In Table 7, ECAR data summary for MC38 WT, MC38 MZ Ctrl., MC38 MZ424 and NIH-3T3 fibroblasts. Represents the % metabolic potential (stressed ECAR/baseline ECAR*100) in terms of ECAR.

The OCR and ECAR values for MC38 cell phenotypes: MC38 WT, MC38 MZ Ctrl. and MC38 MZ424 is higher than NIH-3T3 fibroblasts. A similar metabolic trend was observed in CT26 cell phenotypes. The OCR and ECAR values of CT26 cell variants was higher than NIH-3T3 fibroblasts **[refer fig. (8)].** The OCR based metabolic potential of MC38 WT, MC38 MZ Ctrl. and MC38 MZ424 is 98.76%, 94.18% and 107.58% respectively but for NIH-3T3 fibroblasts is 91.41% **(refer table 6).** The ECAR based metabolic potential of MC38 WT, MC38 MZ Ctrl. and MC38 MZ424 is However in this study, based on the metabolic curve for NIH-3T3 fibroblasts **[refer figs. (9a) and (9b)]** the cells could be metabolically inactive because there is no change in the metabolic curve after the addition of stressor compounds. Moreover, the OCR and ECAR levels for MC38 MZ424 cells are higher than MC38 WT and MC38 MZ Ctrl. cells. Similarly, in case of CT26 cell phenotypes the OCR and ECAR values of CT26 MZ424 cells was higher than CT26 WT and CT26MZ Ctrl cells [**refer figs. (7) and (8)].**

4.4 Cell density optimization of CRC organoids

In order to select the best CRC organoid cell number to develop the EV organoid cell culture and to evaluate the metabolic profile of modified EVs in in-vitro CRC organoid co-culture system, we performed a cell density optimization assay. A day before the

assay, we plated three different cell numbers (50k, 75k and 100k) of CRC organoids in triplicates in the seahorse cell culture 24 well plate and ran the seahorse extracellular flux assay.

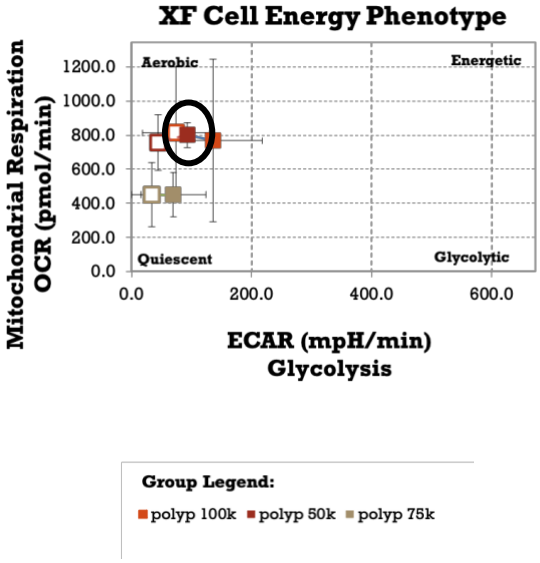

Fig.10: Cell density optimization of CRC organoids. The term 'polyps' denotes mouse CRC organoids. The encircled value represents CRC organoid with a cell number of 50k which was selected for developing the EV organoid co-culture system and for seahorse extracellular flux analysis.

Group name	Baseline OCR/ECAR ratio
polyp 100k	11.00
polyp 50k	**17.01**
polyp 75k	13.43

Table 8: Basal OCR/ECAR ratios of mouse CRC organoids. The highlighted group name represents the baseline OCR/ECAR ratio of mouse CRC organoid group type which was selected for developing the EV organoid co-culture system and for seahorse extracellular flux analysis.

Based on the results, we selected CRC organoids with a cell number of 50k for developing the EV organoid co-culture system and for determining the metabolic changes induced by modified EVs on tumor cells. CRC organoids with a cell number of 50k had the highest baseline OCR/ECAR ratio of 17.01 as compared to CRC organoids with cell numbers 75k and 100k having OCR/ECAR ratios of 13.43 and 11 respectively **[Fig. (10) and refer table 8].**

4.5 Metabolic profiling of EVs derived from CT26 cells phenotypes in CRC organoid co-culture system

To begin with, we isolated the EVs from CT26 cell phenotypes namely CT26 WT cells, CT26 MZ Ctrl and CT26 MZ424 cells. A day before the seahorse extracellular flux assay, we plated 50k CRC organoid cells in triplicates for each of the EVs derived from the CT26 cells phenotypes. We added the EVs from CT26 cell phenotypes to the CRC organoids for developing the EV organoid co-culture system. After 48 hours, we tested the metabolic profile of modified EVs to understand the metabolic changes induced by EVs on CRC organoids and CT26 cell phenotypes.

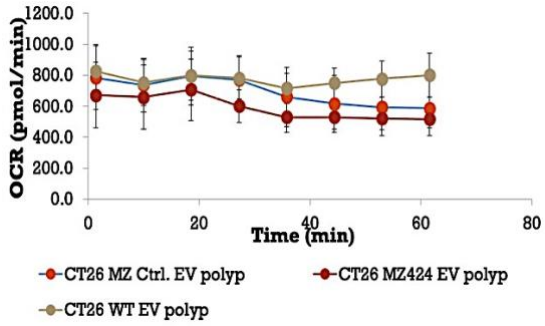

Fig. (11a) OCR metabolic curve for EV CRC organoid co-culture system

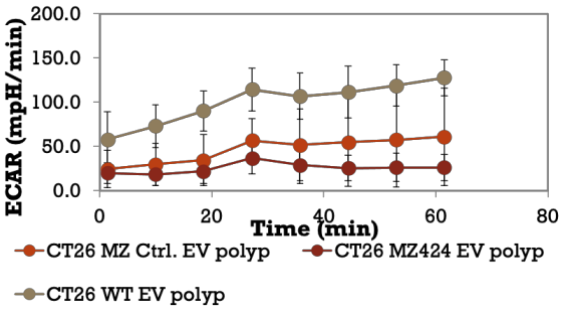

Fig. (11b) ECAR metabolic curve for EV CRC organoid co-culture system

Fig. 11: Metabolic profile of EVs derived from CT26 cell phenotypes co-cultured with CRC organoids

Group Name	Baseline OCR	Baseline OCR StdDev	Stressed OCR	Stressed OCR StdDev	Metabolic Potential (% Baseline OCR)	Metabolic Potential StDev (OCR)
CT26 MZ Ctrl. EV polyp	795.41	185.45	770.95	156.25	97.44	3.82
CT26 MZ424 EV polyp	707.07	198.65	600.79	107.03	87.28	13.64
CT26 MZ424 EV polyp	797.15	159.78	801.17	142.09	100.96	6.12

Table 9: OCR values for EV CRC organoid co-culture system. In Table 9, OCR data summary for CT26 WT, CT26 MZ Ctrl. and CT26 MZ424 EVs co-cultured with CRC organoids. Represents the % metabolic potential (stressed OCR/baseline OCR*100) in terms of OCR.

Group Name	Baseline ECAR	Baseline ECAR StdDev	Stressed ECAR	Stressed ECAR StdDev	Metabolic Potential (% Baseline ECAR)	Metabolic Potential StDev (ECAR)
CT26 MZ Ctrl. EV polyp	34.63	28.83	60.85	55.17	171.20	16.68
CT26 MZ424 EV polyp	22.18	14.40	36.94	17.69	179.19	48.70
CT26 WT EV polyp	90.18	22.62	20.19	20.19	143.79	18.22

Table 10: ECAR values for EV CRC organoid co-culture system. In Table 10, ECAR data summary for CT26 WT, CT26 MZ Ctrl. and CT26 MZ424 EVs co-cultured with CRC organoids. Represents the % metabolic potential (stressed ECAR/baseline ECAR*100) in terms of ECAR.

Figs. (11a) and (11b) depict that OCR and ECAR levels for CT26 MZ424 EVs co-cultured with CRC organoids is lower than CT26 WT and CT26 MZ424 cells co-cultured with CRC organoids. The metabolic potential in terms of OCR for CT26

MZ424 EVs co-cultured with CRC organoids is 87.28% and for CT26 WT EVs and CT26 MZ Ctrl. EVs it is 100.96% and 97.44% respectively **(refer Table 9).** The metabolic potential in terms of ECAR for CT26 MZ424 EVs co-cultured with CRC organoids is 179.19% which is higher than CT26 WT EVs and CT26 MZ Ctrl. CT26 WT and CT26 MZ Ctrl EVs co-cultured with CRC organoids having metabolic potential of 143.79% and 171.20% respectively **(refer Table 10)**.

5. Discussion

Metabolism is a hallmark for cancer. Studying the basic mitochondrial respiratory and glycolytic profile of CRC cells could pave way for investigating new biochemical pathways and developing therapeutic strategies for treating CRC. Firstly, we performed the cell density optimization of two CT26 cell phenotypes and chose 250k as the best cell number with highest baseline OCR/ECAR ratio to proceed with the seahorse extracellular flux assay. Based on previous seahorse assay reports, baseline OCR/ECAR ratio greater than 4 tells us that the cells are utilizing mitochondrial respiration and glycolysis for satisfying their basic energy demands. A baseline OCR/ECAR ratio less than 4 indicates that cells are producing CO_2 and making negligible contribution to metabolism. Moving forward, we evaluated the metabolic profile of CT26 cell phenotypes. Enhanced OCR and ECAR levels of CT26 MZ424 cells tell us that knocking down microRNA 424 induces metabolic changes in this cell line. Similar metabolic trend of CT26 WT cells and CT26 MZ Ctrl. could be seen because of similar phenotypic characteristics of both the cell lines.

In the Warburg phenomenon, cancer cells consume more glucose than surrounding normal cells to satisfy their energy demands. In order to check if our CRC cells demonstrate the Warburg phenotype, we further incorporated a normal cell line i.e. the NIH-3T3 fibroblasts. Our results are consistent with the Warburg phenotype as the CRC cell variants have a higher metabolic activity than NIH-3T3 fibroblasts. In order to evaluate if the metabolic profile of CT26 cell phenotypes is similar to another mouse colon cancer we utilized the MC38 cell phenotype. We observed that MC38 MZ424 cells have enhanced OCR and ECAR levels as compared to the other two MC38 cell variants and MC38 cell variants have a higher metabolic activity than NIH-3T3 fibroblasts. This showed that our data for the metabolism assay for MC38 cells phenotypes is consistent with the data for CT26 cells phenotypes.

Our study reveals that blocking miR424 in CRC cells induces metabolic changes. Our findings are consistent with our hypothesis that knocking down miR424 in CRC cells alter their metabolic profile. This provides avenues for functional validation for altered metabolic pathways triggered after knocking down miR424 in CRC cells which could further yield potential molecular targets for developing treatments for CRC.

Previously, our lab explored the differential gene expression pattern of CT26 and MC38 cell phenotypes. This study was performed by utilizing the RNA seq technique. **Table 11** below comprises a summary of RNA seq data for genes that have an impact on cell metabolism. We chose the top 100 genes from the RNA seq databases with the highest P values, to compare the change in gene expression levels between CRC MZ424 cells and CRC WT as one set and CRC MZ424 and CRC MZ Ctrl. cells as another set.

Cell group	Gene	LogFC	P value	Q value
CT26 MZ424 vs CT26 MZ Ctrl.	Slc6a9	1.1029	4.3197E-06	0.000468135230
	Slc9a9	1.6292	0.000195	0.007825
MC38 MZ424 vs MZ Ctrl.	Slc2a3	2.7431	0.00171	0.0310
MC38 MZ424 vs WT.	Slc2a3	2.2956	0.00455	0.04945

Table 11: Summary of gene expression profiles in CT26 and MC38 cell phenotypes

Table 11 enlists all glucose transporter genes belonging to the slc family. logFC value represents the fold change in the gene expression pattern. Log FC value of approximately 2 or greater means that the gene is upregulated. These results depict that glucose transporter genes are upregulated in CT26 MZ424 and MC38 MZ424 cells as compared to the comparison cell groups.

Our data demonstrates that knocking down miR424 in CRC cells alters their metabolic machinery. A possible mechanism for enhanced OCR and ECAR in CRC MZ424 cells could be **[refer fig. (12)]** that once glucose is oxidized to pyruvate the cell has two

fates: Pyruvate could be further reduced to lactate or pyruvate shuttles through the Kreb's cycle, both the reactions ultimately produce ATP for the cell to survive.

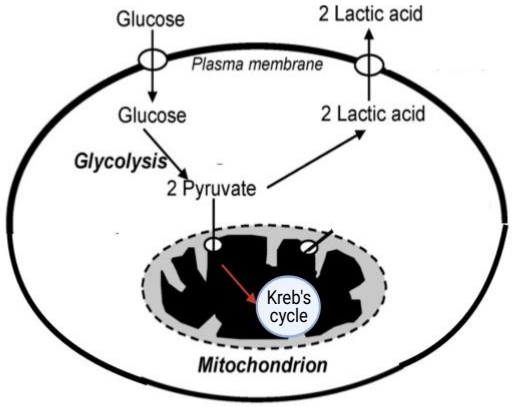

Fig. 12: Potential mechanism for enhanced OCR and ECAR in CRC MZ424 cells

We have some supporting data **(refer table 11)** that indicates upregulation of glucose transporter genes in CRC MZ424 cells as compared to CRC WT and CRC MZ Ctrl. This provides further explanation for enhanced mitochondrial respiration and glycolysis in CRC MZ424 cells.

In order to gain information on how modified EVs affect metabolism in CRC microenvironment and the effect of their metabolism on CRC cells, we developed an *in-vitro* EV CRC organoid co-culture system. We noticed that modified EVs co-cultured with mouse CRC organoids showed lower metabolic activity as compared to CT26 WT EVs and CT26 MZ Ctrl. EVs co-cultured with mouse CRC organoids. We propose a potential mechanism for this: when modified EVs release anti-miR424 into the CRC organoids, the glucose transporter genes **(refer table 11, CT26 MZ424 *vs* MZ Ctrl. section)** could be downregulated which could yield decreased OCR (mitochondrial respiratory) and ECAR (glycolytic) levels of modified EVs. These results are in conjunction with our former experiment which demonstrated that CT26 MZ424 cells (CT26 cells expressing anti-miR424) possess elevated levels of glucose transporter genes **[refer fig. 7 and table 11]**. We believe that the glucose transporter genes **(enlisted in table 11, CT26 MZ424 *vs* MZ Ctrl. section)** could be the indirect targets of miR-424.

6. Limitations

There are certain inadequacies in our study which was performed to evaluate the effect of modified EVs on CRC cell metabolism. To understand the metabolic function of CRC cell phenotypes more, a control consisting of miR424 overexpressing CRC cells could have been incorporated in the study. Our study utilized only one time point (24 hrs) to look at the metabolic profile of CRC cell phenotypes. The metabolic profile of CRC cells could have been studied at different time points (2 hours, 4 hours, 6 hours, 48 hours, 72 hours). While studying the metabolic profile of modified EVs in EV organoid co-culture system, matrigel (required for organoid solidification) could have been incorporated as a negative control. While developing the EV organoid co-culture system, EVs could be exposed to mouse CRC organoids for a longer duration of time (3 days,4 days,1 week) to further study the metabolic changes induced by modified EVs.

7. Future Directions

Further studies could be conducted to understand the metabolic reprogramming induced by blocking the immunosuppressive miR424 in CRC cells and the effect of modified EVs metabolism on tumor cells. In order to confirm if the miR424 knocked down CRC cells produce lactate look at the function of lactate dehydrogenase (LDHA) and monocarboxylate transporter (MCT) genes using enzyme kinetic assays. EV synthesis in mouse CRC organoids could be blocked by treating these organoids with GW4869 drug. These organoids could be further co-cultured with CRC EV phenotypes to study the metabolic changes induced by modified EVs in in-vitro CRC organoid system and tumor cells.

Chapter 2: Biodistribution of Modified Extracellular Vesicles in an *in-vivo* tumor model

8. Introduction

In this chapter, we will review the previous research studies conducted to study the biodistribution profile of EVs in tumor bearing mouse models. Furthermore, this section discusses about the therapeutic potential and biodistribution of our modified EVs in an *in-vivo* tumor model.

8.1 Biodistribution of exosomes in *in-vivo* tumor model

In order to determine the therapeutic efficacy of EVs it is crucial to gain insights into their biodistribution and pharmacokinetic profile. Several labelling and imaging techniques have been developed to track exosomes in vivo. Bioluminescence imaging (BLI) and fluorescence imaging (FLI) are two major methods used in detecting EVs within the visible light spectrum (390–700 nm) [33]. Bioluminescent imaging is a protein based labelling method wherein plasmid transfection or lentiviral transduction can be performed for EVs to express luciferase for imaging. Takahashi et al. demonstrated that *Gaussia* luciferase (Gluc) fused between a secretion signal peptide and C1C2 domain of lactadherin could be labelled onto EV membrane [34]. Fluorescent protein- and organic dye-based labelling are used to enable FLI EV imaging with excellent spatial resolution [33]. Organic dyes bind fluorophores with different functional groups to label the lipid bilayer or proteins of interest on EVs. DiR and DiD are lipophilic dyes and exhibit a strong fluorescent signal when incorporated into the cytosol [33,35]. Other clinical imaging techniques presently being explored for EV imaging are single photon emission computed tomography (SPECT), Positron Emission Tomography (PET) and Magnetic Resonance Imaging (MRI).

Several studies have examined the biodistribution of EVs in tumor bearing mouse models. The cell source, route of administration and dose of EVs impacts their biodistribution pattern in different organs. One of the studies [36], combined Gaussia luciferase and metabolic biotinylation to create a sensitive EV reporter (EV-GlucB) for monitoring EVs via multimodal imaging, in tumor bearing mouse tissue samples. Bioluminescence and fluorescence mediated tomography imaging on mice displayed a

predominant localization of intravenously administered EVs in spleen and liver and systemic administration of EVs showed localization in tumor tissue after an hour [36]. Smyth et.*al* and colleagues explored the biodistribution profile of TEVs extracted from 4T1, MCF-7, and PC3 cell supernatants and found that EVs accumulate in the liver, spleen and tumor tissues [37].

The molecular mechanisms of organotropism of exosomes is elusive. Not all cell sources produce EVs that have tumor homing properties. However, certain tumor-homing exosomes could be utilized as targeted delivery vehicles [38]. EVs derived from mesenchymal stem cells (MSC) have been identified to exhibit tumor homing properties [38,39]. The tumor homing property of MSC EVs have been successfully exploited to deliver therapeutic miRNAs [40].

9. Rationale and Aim

Previous research in our lab has demonstrated that, EVs without immunosuppressive miR-424 (modified EVs) enhanced the anti-tumour response in CRC tumor mouse model and paves way for developing novel therapeutic strategies [32]. Presently, attributes such as EV tissue distribution, clearance and blood levels of EVs are under investigation [36]. These parameters are critical for establishing the therapeutic efficacy and potential toxicity of our modified EVs. Information regarding biodistribution profile of modified EVs will aid in determining their dose and therapeutic window. Our objective in this study is to evaluate the biodistribution profile of modified EVs using a tumor bearing mouse model.

10. Material and methods

10.1 Cell Culture

Murine colon cancer cell line CT26 transduced with anti-miR424 (CT26-MZ424) lentiviral vector (SIGMA-ALDRICH) was previously established in the lab. CT26-MZ424 cells were maintained in RPMI 1640 media supplemented with 10% FBS and 1% antibiotics.

10.2 Modified EV labelling

Isolated modified EVs were labelled using lipophilic tracer DiO dye. Briefly, modified EVs were incubated with 1.5uL DiO/20µg modified EVs in 100µL PBS. Excess dye was removed by washing the sample thrice with PBS at 100000g for 70 mins utilizing the ultracentrifuge. The final pellet was resuspended in 100 µL PBS and the protein concentration was measured using microBCA assay (Thermo Fisher Scientific).

10.3 Modified EV characterization

10.3.1 Modified EV size determination

Modified EVs size was determined using a nanoparticle tracking analyzer (NanoSight LM-10). Samples of EVs were diluted with PBS to reach a volume of 500 µL, then infused into the NanoSight machine using a syringe. Data was collected in quintuplicate, then analyzed using NanoSight software.

10.4 Mice

8-10 week old miR322/424 KO BALB/C mice (from Jackson lab) were used for the study. All animal procedures were conducted in accordance with the University of Minnesota regulations on the use of experimental animals and approved by IACUC.

10.5 Subcutaneous tumor mouse model

To establish the subcutaneous mouse model, we injected 0.2 x 10^6 CT26 WT cells that were resuspended in 50 µL RPMI 1640 media (with 10% FBS and 1% antibiotics) and 50µL Matrigel (BD Biosciences) to the right flank of miR322/424 KO BALB/C mice. The mice were monitored for 2 weeks for tumor growth.

10.6 *Ex-vivo* animal study

A dose of 20µg of modified EVs were injected to the animal via tail vein. Animal was euthanized after 30 minutes of injection. The tissues from heart, lung, liver, spleen and tumor were collected for single cell suspension preparation.

10.7 Flow cytometry analysis

In order to prepare single cell suspensions, the tissues obtained from heart, lung and tumor were minced and were digested using collagenase IV (Thermo Fisher Scientific) and DNAse I (New England Biolabs) by shaking at 37°C. Liver was added to the isolation buffer (consisting of 4% BSA, 2mM EDTA in HBSS) and digested using DNAseI and digestion mixture (5000 U/mL collagenase IV in CLICKS/EHAA medium) by shaking at 37°C. All tissues were passed through 70µm strainer and then treated with RBC lysis buffer for 15 minutes at room temperature. From each suspension, $2x10^6$ cells were stained with zombie aqua dye for viability. Flow cytometric analysis of these samples was performed using the BD FACS Canto II Analyzer and analysis was performed using FlowJo software (version 10.6.1).

11. Results

11.1 Modified EV Characterization

Modified EVs were characterized based on size using Nanotracking analyzer (NTA). The NTA curve depicts the average particle size of modified EVs with a peak at 136 nm **[refer fig. (13)].** The average size distribution of unlabelled modified EVs was 150.6 +/-5.2 nm.

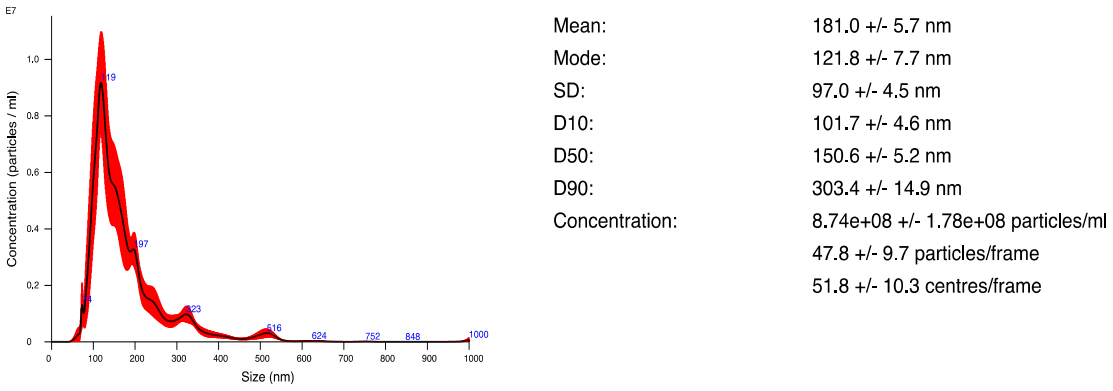

Fig. 13: Nanotracking analysis of modified EVs

11.2 Modified EV labelling

Before modified EV labelling, EVs were isolated from CT26 MZ424 cells as per the protocol described in **section 3.4**. Previously, DiO to EV ratio was standardized to be 20µg modified EVs/100µL PBS in our lab. To confirm if the modified EVs are labelled correctly, the modified EVs were incubated with CT26 WT cells overnight after 3x washes. For comparison, we added 1.5µL DiO in 100 µL PBS and incubated this solution with CT26 WT cells overnight. To check if CT26 WT cells can uptake the DiO dye.

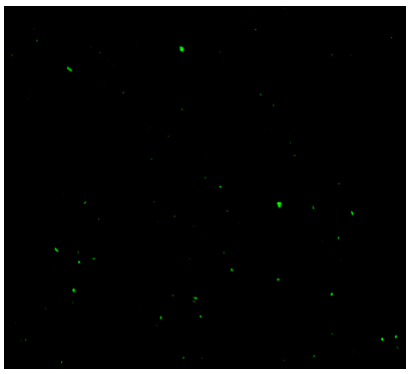

Fig (14a): DiO-only samples incubated CT26-WT cells (3x washes)

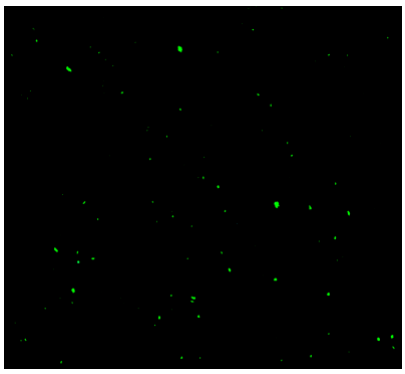

Fig (14b): DiO labelled CT26 MZ424 EVs incubated with CT26-WT cells (3x washes)

Fig. 14: Labelling of modified EVs

Fig. (14a) depicts that CT26 WT cells uptake the DiO dye. In **fig. (14b)**, presence of GFP positive CT26 WT cells confirms that modified EVs have been labelled with the DiO dye.

11.3 Biodistribution of DiO labelled modified EVs

After administration of modified EVs via tail vein injection, we examined the biodistribution of modified EVs in a tumor bearing mouse model. Data generated from one tumor bearing mouse was utilized for the analysis. 20µg of modified EVs were injected and spleen, liver, lung, tumor and heart tissues were collected from the mouse.

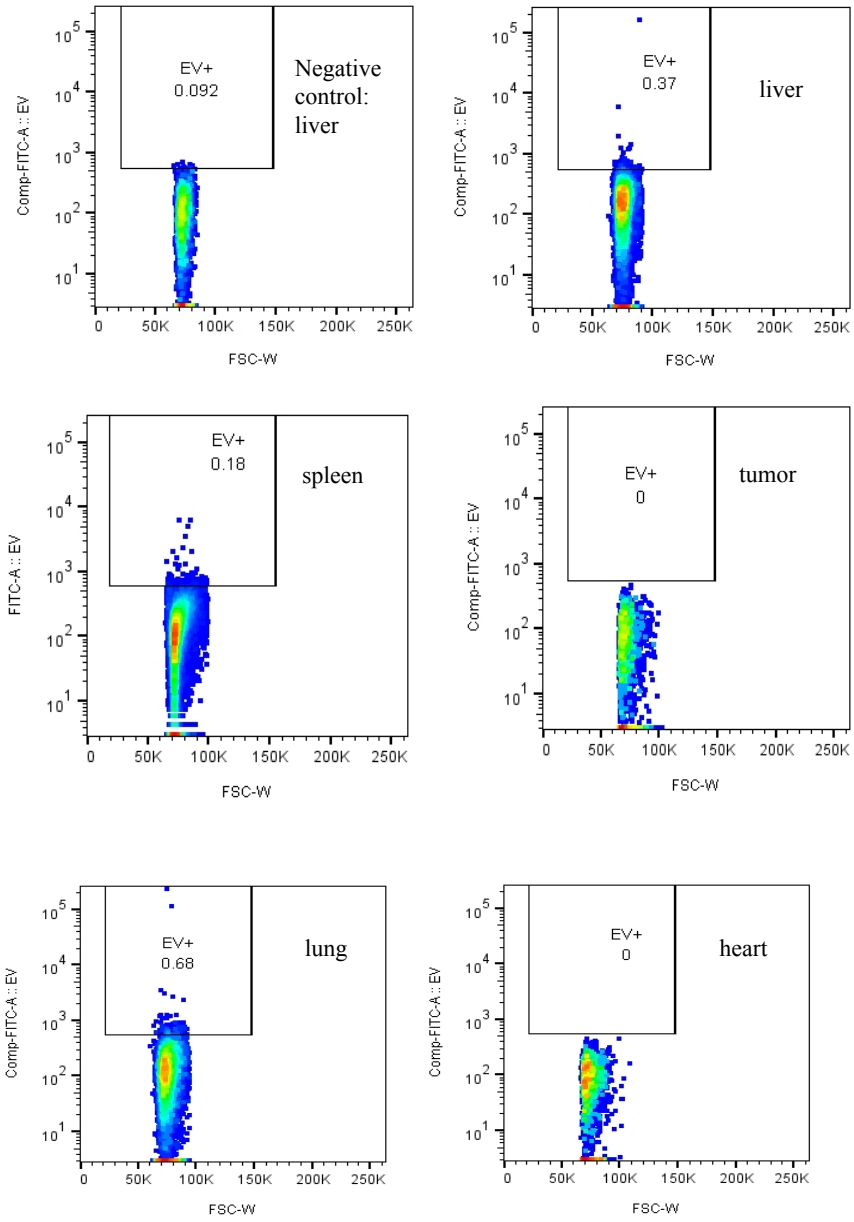

Fig. 15: Flow cytometry plots of liver, spleen, tumor, lung and heart

We collected five tissues from tumor bearing animals to look at the percentage of cells which capture modified EV positive signal. The lung shows the highest percentage of modified EV positive signal of 0.68% **[refer fig.(15)].** Followed by spleen and liver, which show a modified EV positive signal of 0.18% and 0.37% respectively **[refer fig.(15)].** Heart and tumor did now show any modified EV positive signal **[refer fig.(15)]**.

12. Discussion

EVs have been emerging as target agents for treating cancer. Our study aimed at determining the biodistribution profile of modified EVs in a tumor bearing mouse model. EVs have an average size range of 30-200 nm. Our modified EVs have an average size distribution of 150.6 +/-5.2 nm which validates the presence of modified EVs in our sample. DiO labelled modified EVs were incubated with CT26 WT cells overnight because a low resolution fluorescence microscope was utilized for confirming if the modified EVs were labelled. Presence of GFP positive signal in CT26 WT cells incubated with DiO labelled modified EVs reveals that modified EVs have been labelled correctly.

Our biodistribution study utilizing *in-vivo* tumor model revealed that cells in the lung captured the highest percentage of EV positive signal followed by spleen and liver. These organs are of importance in CRC since liver and lung are the major metastatic sites of CRC and in the spleen where the host immune response is activated. This data is consistent with our hypothesis that modified EVs show predominant biodistribution in liver and lungs. However, there was no EV positive signal shown by cardiomyocytes. Moreover, there was absence of EV positive signal in tumor cells.

Our lab has previously explored the biodistribution profile of modified EVs in normal mouse model and orthotopic mouse model. **Table 12** below represents the comparison of biodistribution profiles of modified EVs in normal mouse model and tumor bearing mouse model.

Tissue type	Normal mouse model (% of EV positive cells)	Tumor mouse model (% of EV positive cells)
Liver	0.96 0.31 0.29	0.68
Average	3.15e-3	-
Spleen	0.18 0.051 3.03e-3 9.02e-4	0.18
Average	5.87e-2	-
Tumor	-	0.24 (orthotopic mouse model) 0% (SC tumor mouse model)
Lung	0.24 0.17 1.17e-3	0.68
Average	0.137	-
Heart	0 0 6.26 16.2	0
Average	5.62	-

Table 12: Summary of biodistribution profile of modified EVs in normal and tumor bearing mouse model

Tumor bearing mouse model shows higher biodistribution of modified EVs in liver, spleen and lung as compared to normal mouse model **(refer table 12).** Heart shows no biodistribution in tumor bearing mouse model but shows an average EV positive signal of 5.62% in cardiomyocytes from normal mouse model **(refer table 12).** In the orthotopic mouse model tumor cells show an EV positive signal of 0.24% but there is no EV positive signal in the tumor cells isolated from SC tumor mouse model **(refer table 12).** This requires further investigation in terms of determining the tumor homing properties of modified EVs.

13. Limitations

There are certain limitations in our modified EV biodistribution study which was conducted utilizing an *in-vivo* tumor model. A negative control (PBS injection) in tumor bearing mice could be incorporated to compare the biodistribution profile of modified EVs in different tissues. The biodistribution pattern of modified EVs could be examined in other tissues such as kidneys, GI tract, lymph nodes, bone marrow, muscle, brain and muscle. The clearance measurements of modified EVs could be investigated in blood, serum and plasma. More optimization of the study could be done by utilizing more tumor bearing mice sample sets to study the variation of EV positive signal for the tissues in different tumor bearing mice sample sets.

14. Future directions

Further studies are required for understanding the biodistribution profile of modified EVs in tumor bearing mouse model. An experiment to compare the modified EV biodistribution profile at different time points (5 min,10 min, 1 hr, 2 hrs) could be done. An experiment involving IP administration of modified EVs in tumor bearing mice could be performed. The data for biodistribution profile of modified EVs via IP injection could be compared with pre-existing tail vein injection data for defining the preferred route for administering modified EVs to the tumor bearing mouse. More tumor mouse models are required to validate our result and to perform statistical comparison of the modified EVs biodistribution profile between normal and tumor-bearing animal models. Orthotopic mouse models could be generated for studying the biodistribution profile of modified EVs in a CRC mouse model.

References

[1] Rak J and Guha A 2012 Extracellular vesicles - vehicles that spread cancer genes *BioEssays* **34** 489–97

[2] Głuszko A, Szczepański M J, Ludwig N, Mirza S M and Olejarz W 2019 Exosomes in Cancer: Circulating Immune-Related Biomarkers *Biomed Res. Int.* **2019**

[3] Natalya N. Pavlova and Craig B. Thompson 2018 Emerging metabolic hallmarks of cancer *Physiol. Behav.* **176** 139–48

[4] Yang E, Wang X, Gong Z, Yu M, Wu H and Zhang D 2020 Exosome-mediated metabolic reprogramming: the emerging role in tumor microenvironment remodeling and its influence on cancer progression *Signal Transduct. Target. Ther.* **5** 1–13

[5] Silva-Almeida C, Ewart M A and Wilde C 2020 3D gastrointestinal models and organoids to study metabolism in human colon cancer *Semin. Cell Dev. Biol.* **98** 98–104

[6] Zhou X, Xie F, Wang L, Zhang L, Zhang S, Fang M and Zhou F 2020 The function and clinical application of extracellular vesicles in innate immune regulation *Cell. Mol. Immunol.* **17** 323–34

[7] Mathieu M, Martin-Jaular L, Lavieu G and Théry C 2019 Specificities of secretion and uptake of exosomes and other extracellular vesicles for cell-to-cell communication *Nat. Cell Biol.* **21** 9–17

[8] Xiao Y, Zhong J, Zhong B, Huang J, Jiang L, Jiang Y, Yuan J, Sun J, Dai L, Yang C, Li Z, Wang J and Zhong T 2020 Exosomes as potential sources of biomarkers in colorectal cancer *Cancer Lett.* **476** 13–22

[9] Shields S B, Oestreich A J, Winistorfer S, Nguyen D, Payne J A, Katzmann D J and Piper R 2009 ESCRT ubiquitin-binding domains function cooperatively during MVB cargo sorting *J. Cell Biol.* **185** 213–24

[10] Christ L, Wenzel E M, Liestøl K, Raiborg C, Campsteijn C and Stenmark H 2016 ALIX and ESC RT-I/II function as parallel ESC RT-III recruiters in

cytokinetic abscission *J. Cell Biol.* **212** 499–513

[11] Latifkar A, Ling L, Hingorani A, Johansen E, Clement A, Zhang X, Hartman J, Fischbach C, Lin H, Cerione R A and Antonyak M A 2019 Loss of Sirtuin 1 Alters the Secretome of Breast Cancer Cells by Impairing Lysosomal Integrity *Dev. Cell* **49** 393-408.e7

[12] Yoon S, Kovalenko A, Bogdanov K and Wallach D 2017 MLKL, the Protein that Mediates Necroptosis, Also Regulates Endosomal Trafficking and Extracellular Vesicle Generation *Immunity* **47** 51-65.e7

[13] Wei Y, Wang D, Jin F, Bian Z, Li L, Liang H, Li M, Shi L, Pan C, Zhu D, Chen X, Hu G, Liu Y, Zhang C Y and Zen K 2017 Pyruvate kinase type M2 promotes tumour cell exosome release via phosphorylating synaptosome-associated protein 23 *Nat. Commun.* **8**

[14] Blanc L and Vidal M 2018 New insights into the function of Rab GTPases in the context of exosomal secretion *Small GTPases* **9** 95–106

[15] Yue B, Yang H, Wang J, Ru W, Wu J, Huang Y, Lan X, Lei C and Chen H 2020 Exosome biogenesis, secretion and function of exosomal miRNAs in skeletal muscle myogenesis *Cell Prolif.* **53** 1–10

[16] El Andaloussi S, Mäger I, Breakefield X O and Wood M J A 2013 Extracellular vesicles: Biology and emerging therapeutic opportunities *Nat. Rev. Drug Discov.* **12** 347–57

[17] Daassi D, Mahoney K M and Freeman G J 2020 The importance of exosomal PDL1 in tumour immune evasion *Nat. Rev. Immunol.* **20** 209–15

[18] Raposo G, Nijman H W, Stoorvogel W, Leijendekker R, Harding C V., Melief C J M and Geuze H J 1996 B lymphocytes secrete antigen-presenting vesicles *J. Exp. Med.* **183** 1161–72

[19] Lucchetti D, Tenore C R, Colella F and Sgambato A 2020 Extracellular Vesicles and Cancer : A Focus on 1–19

[20] Brown R E, Short S P and Williams C S 2018 Colorectal Cancer and Metabolism *Curr. Colorectal Cancer Rep.* **14** 226–41

[21] Fisel P, Schaeffeler E and Schwab M 2018 Clinical and Functional Relevance of the Monocarboxylate Transporter Family in Disease Pathophysiology and

Drug Therapy *Clin. Transl. Sci.* **11** 352–64

[22] Li T, Copeland C and Le A 2021 Glutamine Metabolism in Cancer *Adv. Exp. Med. Biol.* **1311** 17–38

[23] Ryall J G, Cliff T, Dalton S and Sartorelli V 2015 Metabolic Reprogramming of Stem Cell Epigenetics *Cell Stem Cell* **17** 651–62

[24] Ward, S P and Thompson, B C 2013 Metabolic Reprogramming: A Cancer Hallmark Even Warburg Did Not Anticipate *Cancer Cell* **21** 297–308

[25] Zheng J 2012 Energy metabolism of cancer: Glycolysis versus oxidative phosphorylation (review) *Oncol. Lett.* **4** 1151–7

[26] Hagland H R and Søreide K 2015 Cellular metabolism in colorectal carcinogenesis: Influence of lifestyle, gut microbiome and metabolic pathways *Cancer Lett.* **356** 273–80

[27] Beckler M D, Higginbotham J N, Franklin J L, Ham A J, Halvey P J, Imasuen I E, Whitwell C, Li M, Liebler D C and Coffey R J 2013 Proteomic analysis of exosomes from mutant KRAS colon cancer cells identifies intercellular transfer of mutant KRAS *Mol. Cell. Proteomics* **12** 343–55

[28] Wang X, Zhang H, Yang H, Bai M, Ning T, Deng T, Liu R, Fan Q, Zhu K, Li J, Zhan Y, Ying G and Ba Y 2020 Exosome-delivered circRNA promotes glycolysis to induce chemoresistance through the miR-122-PKM2 axis in colorectal cancer *Mol. Oncol.* **14** 539–55

[29] La Shu S, Yang Y, Allen C L, Maguire O, Minderman H, Sen A, Ciesielski M J, Collins K A, Bush P J, Singh P, Wang X, Morgan M, Qu J, Bankert R B, Whiteside T L, Wu Y and Ernstoff M S 2018 Metabolic reprogramming of stromal fibroblasts by melanoma exosome microRNA favours a pre-metastatic microenvironment *Sci. Rep.* **8** 1–14

[30] Bas T and Augenlicht L H 2014 Real time analysis of metabolic profile in Ex vivo mouse intestinal crypt organoid cultures *J. Vis. Exp.* 1–5

[31] Technologies A 2017 Agilent Seahorse XF Cell Energy Phenotype Test Kit 20

[32] Zhao X, Yuan C, Wangmo D and Subramanian S 2021 Tumor-Secreted Extracellular Vesicles Regulate T-Cell Costimulation and Can Be Manipulated To Induce Tumor-Specific T-Cell Responses *Gastroenterology* 612–26

[33] Chuo S T Y, Chien J C Y and Lai C P K 2018 Imaging extracellular vesicles: Current and emerging methods *J. Biomed. Sci.* **25** 1–10

[34] Takahashi Y, Nishikawa M, Shinotsuka H, Matsui Y, Ohara S, Imai T and Takakura Y 2013 Visualization and in vivo tracking of the exosomes of murine melanoma B16-BL6 cells in mice after intravenous injection *J. Biotechnol.* **165** 77–84

[35] Heinrich L, Freyria A M, Melin M, Tourneur Y, Maksoud R, Bernengo J C and Hartmann D J 2007 Confocal laser scanning microscopy using dialkylcarbocyanine dyes for cell tracing in hard and soft biomaterials *J. Biomed. Mater. Res. - Part B Appl. Biomater.* **81** 153–61

[36] Lai C P, Mardini O, Ericsson M, Prabhakar S, Maguire C A, Chen J W, Tannous B A and Breakefield X O 2014 Dynamic biodistribution of extracellular vesicles in vivo using a multimodal imaging reporter *ACS Nano* **8** 483–94

[37] Smyth T, Kullberg M, Malik N, Smith-Jones P, Graner M W and Anchordoquy T J 2015 Biodistribution and delivery efficiency of unmodified tumor-derived exosomes *J. Control. Release* **199** 145–55

[38] Yi Y W, Lee J H, Kim S Y, Pack C G, Ha D H, Park S R, Youn J and Cho B S 2020 Advances in analysis of biodistribution of exosomes by molecular imaging *Int. J. Mol. Sci.* **21**

[39] Lourenco S, Teixeira V H, Kalber T, Jose R J, Floto R A and Janes S M 2015 Macrophage Migration Inhibitory Factor–CXCR4 Is the Dominant Chemotactic Axis in Human Mesenchymal Stem Cell Recruitment to Tumors *J. Immunol.* **194** 3463–74

[40] Mendt M, Kamerkar S, Sugimoto H, McAndrews K M, Wu C C, Gagea M, Yang S, Blanko E V R, Peng Q, Ma X, Marszalek J R, Maitra A, Yee C, Rezvani K, Shpall E, LeBleu V S and Kalluri R 2018 Generation and testing of clinical-grade exosomes for pancreatic cancer *JCI insight* **3** 1–22